Environ. Sci. Technol. **2004**, *38,* 5591−5597

Cryogenic Laser Induced Fluorescence Characterization of U(VI) in Hanford Vadose Zone Pore Waters

ZHEMING WANG,* JOHN M. ZACHARA, WASSANA YANTASEE, PAUL L. GASSMAN, CHONGXUAN LIU, AND ALAN G. JOLY

Pacific Northwest National Laboratory, Richland, Washington 99352

Ambient and liquid helium temperature laser-induced time-resolved uranyl fluorescence spectroscopy was applied to study the speciation of aqueous uranyl solutions containing carbonate and phosphate and two porewater samples obtained by ultracentrifugation of U(VI)-contaminated sediments. The significantly enhanced fluorescence signal intensity and spectral resolution found at liquid helium temperature allowed, for the first time, direct fluorescence spectroscopic observation of the higher aqueous uranyl complexes with carbonate: $UO_2(CO_3)_2^{2-}$, $UO_2(CO_3)_3^{4-}$, and $(UO_2)_2(OH)_3CO_3^-$. The porewater samples were nonfluorescent at room temperature. However, at liquid helium temperature, both porewater samples displayed strong, well-resolved fluorescence spectra. Comparisons of the spectroscopic characteristics of the porewaters with those of the standard uranyl−carbonate complexes confirmed that U(VI) in the porewaters existed primarily as $UO_2(CO_3)_3^{4-}$ along with a small amount of other minor components, such as dicalcium−urano−tricarbonate complex, $Ca_2UO_2(CO_3)_3$, consistent with thermodynamic calculation. The U(VI)−carbonate complex is apparently the mobile species responsible for the subsurface migration of U(VI), even though the majority of the in-ground U(VI) inventory at the site from which the samples were obtained exists as intragrain U(VI)−silicate precipitates.

Introduction

The aqueous complexation of uranium(VI) by carbonate and phosphate is an important factor in the risk assessment and formulation of decontamination strategies for the remediation of uranium contaminated soils and sediments. Both carbonate and phosphate form an array of solid uranium minerals as well as binary and ternary complexes involving other ligands such as the hydroxide ions in aqueous solution or as adsorbates at the mineral/metal−oxide surface (*1*−*5*). However, the solubilities of U(VI) complexes with phosphate and carbonate differ dramatically, with U(VI)−carbonate complexes being the most soluble ones and U(VI)−phosphate complexes among the least soluble ones in natural waters (*6*−*8*). As such, the results of thermodynamic simulation and transport modeling suggest that under circumneutral to weakly basic conditions U(VI)−carbonate and/or U(VI)−hydroxo−carbonate complexes dominate in natural waters and thus are likely to be responsible for the transport and migration of U(VI) in the subsurface (*9*, *10*). In contrast, the low solubilities of U(VI) phosphate complexes have encouraged the studies of phosphate minerals as U(VI) migration barriers (*11*, *12*).

While some natural U(VI)−carbonate and −phosphate minerals have been identified and characterized (*3*, *4*, *13*) and a relatively complete thermodynamic database for U(VI)−carbonate and −phosphate complexes in aqueous solutions has been compiled (*1*), there has been limited direct spectroscopic evidence for U(VI)−carbonate/phosphate species in contaminated soils and sediments and in natural waters (*7*, *9*, *14*). Uranyl−phosphate complexes are important in weakly acidic sediments. Fluorescence and Raman spectroscopic measurements have identified that meta-autunite, phosphuranylite, and uranyl hydroxide (schoepite) are the primary U(VI) precipitates in uranium-contaminated soils and sediments at the U.S. DOE Fernald site (*15*). The aqueous speciation of U(VI) will exert major influence on how it partitions to the solid phase (*9*, *16*−*18*). A detailed solution phase characterization in such media not only determines the mobile component but also allows estimation of the type of surface complexation reactions that may occur on mineral surfaces.

The concentration of U(VI) is typically on the order of 10^{-7} M or lower in groundwaters and 10^{-5} M in mining waters (*19*, *20*). These concentrations are below the detection limit of many spectroscopic techniques such as IR, FTIR, Raman, XRD, and EXAFS. The most sensitive current technique for the analysis of dilute U(VI) solutions is fluorescence spectroscopy using high power, pulsed lasers and time-resolved detection systems (*21*). The intensity, bandwidth, and spacing of the vibronic bands of the uranyl fluorescence spectra and its fluorescence lifetime are highly sensitive to the bonding, symmetry, and local chemical environment of uranyl ion and thus provide useful tools for the study of uranyl speciation (*22*, *23*). Uranyl fluorescence measurements have confirmed the formation of aqueous uranyl complexes with simple ligands such as nitrate (1:1), sulfate (1:1 and 1:2) (*24*), silicate (1:1) (*25*), carbonate (1:1) (*2*), phosphate (1:1) (*26*), and hydroxide (1:1) (*27*). A combination of fluorescence and UV−visible spectroscopic measurements have identified the dinuclear hydroxo species, $(UO_2)_2(OH)_2^{2+}$, and the trinuclear hydroxo species, $(UO_2)_3(OH)_5^+$ (*28*, *29*). Recently, it was reported that in the presence of high levels of Ca^{2+}, the dicalcium−uranyl−tricarbonate complex was present in seepage waters as identified by fluorescence spectroscopy (*14*). Subsequent research has indicated that the $Ca_2[UO_2(CO_3)_3]$ complex is the predominant, thermodynamically stable species at pH 8 and above in calcium rich, oxic water (*30*). Under ambient conditions, thermodynamic calculations indicate that uranyl−carbonate complexes dominate U(VI) speciation from pH 6 to 10. Unfortunately, the quenching effect of carbonate (*31*) has hindered the fluorescence spectroscopic observation of the higher uranyl−carbonate complexes, $(UO_2)(CO_3)_2^{2-}$ and $(UO_2)(CO_3)_3^{3-}$, as well as the mixed ligand complex, $(UO_2)_2(OH)_3CO_3^-$ (*2*, *32*).

We have recently demonstrated that at near-liquid helium temperature (LHeT) the intensity and resolution of the fluorescence spectra of uranyl−silicate minerals could be significantly improved, making it possible to identify these phases in Hanford vadose zone sediments (*33*). Here, we have extended that technique to characterize a series of aqueous uranyl−carbonate solutions, one phosphate-

* Corresponding author phone: (509)376-6119; fax: (509)376-3650; e-mail: Zheming.Wang@pnl.gov. Corresponding author address: Pacific Northwest National Laboratory, MSIN K8-96, P.O. Box 999, Richland, WA 99352.

10.1021/es049512u CCC: $27.50 © 2004 American Chemical Society
Published on Web 09/25/2004

TABLE 1. Solution Composition of Aqueous Uranyl−Carbonate Complexes at 25 °C, I = 0.1 M

sample no.	pH	pCO_2 (atm)	[U(VI)] (M)	dominant aqueous species
		Uranyl Carbonates		
1	2.6	$10^{-3.5}$	5×10^{-5}	100% UO_2^{2+}
2	4.70	1	5.0×10^{-6}	14% UO_2^{2+}, 66% UO_2CO_3, 16% $(UO_2)_2(OH)_3CO_3^-$
3	4.80	1	2.0×10^{-6}	10% UO_2^{2+}, 74% UO_2CO_3, 6% $UO_2(CO_3)_2^{2-}$, 10% $(UO_2)_2(OH)_3CO_3^-$
4	5.90	1	2.0×10^{-6}	6% UO_2CO_3, 86% $UO_2(CO_3)_2^{2-}$, 7% $UO_2(CO_3)_3^{4-}$
5	7.00	$10^{-3.5}$	1.0×10^{-5}	100% $(UO_2)_2(OH)_3CO_3^-$
6	10.59	1	5.0×10^{-6}	100% $UO_2(CO_3)_3^{4-}$
7	8.60 with 0.005 M Ca^{2+}	$10^{-3.5}$	1.0×10^{-5}	100% $Ca_2UO_2(CO_3)_3$
		Uranyl Phosphate		
10a	2.5	$[PO_4^{3-}] = 0.002$ M	2.0×10^{-5}	100% $UO_2(HPO_4)_2^{2-}$

TABLE 2. Formation Constants for Aqueous U(VI) Complexes at 25 °C, and I = 0

reaction	log K	source[a]
$UO_2^{2+} + H_2O = UO_2OH^+ + H^+$	−5.2	1
$UO_2^{2+} + 2H_2O = UO_2(OH)_2(aq) + 2H^+$	−12.0	1
$UO_2^{2+} + CO_3^{2-} = UO_2CO_{3(aq)}$	9.68	1
$UO_2^{2+} + 2CO_3^{2-} = UO_2(CO_3)_2^{2-}$	16.94	1
$UO_2^{2+} + 3CO_3^{2-} = UO_2(CO_3)_3^{4-}$	21.60	1
$2UO_2^{2+} + CO_3^{2-} + 3\,H_2O = (UO_2)_2CO_3(OH)_3^- + 3H^+$	−0.86	1
$UO_2^{2+} + PO_4^{3-} = UO_2PO_4^-$	13.23	1
$UO_2^{2+} + PO_4^{3-} + H^+ = UO_2HPO_{4(aq)}$	19.59	1
$UO_2^{2+} + PO_4^{3-} + 2H^+ = UO_2H_2PO_4^+$	22.82	1
$UO_2^{2+} + 2H^+ + 2PO_4^{3-} = UO_2(HPO_4)_2^{2-}$	42.99	1
$UO_2^{2+} + H_4SiO_4 = UO_2H_3SiO_4^+ + H^+$	1.60	2
$UO_2^{2+} + 2Ca^{2+} + 3CO_3^{2-} = Ca_2UO_2(CO_3)_{3(aq)}$	29.8	3

[a] 1. ref *1*; 2. ref *34* after correction for activity using Davis equation; 3. ref *30*.

containing solution, and two porewaters extracted from Hanford vadose zone sediment. At LHeT, all the complexes displayed strong, well-resolved fluorescence emission spectra. A comparison of the spectra of the Hanford vadose zone pore waters with those of the standard uranyl−carbonate/phosphate complexes confirmed that the Hanford vadose zone pore waters contained mainly 1:3 uranyl−carbonate complexes.

Experimental Section

Sample Preparations. *Aqueous Uranyl−Carbonate/Phosphate Solutions.* A set of standard U(VI)−carbonate solutions were designed and synthesized to assist in the identification of aqueous U(VI) species in the sedimentary porewater samples. Specific solution conditions (pH, CO_2 partial pressure, and concentrations of reactants) were selected where only one or two aqueous species were expected to dominate based on thermodynamic calculation. Such conditions were identified by equilibrium speciation calculations (Table 1) using the MINTEQA2 and/or MINEQL+ software with the most current, critically reviewed thermodynamic stability constants for the uranyl complexes (Table 2) (*1*, *30*, *34*). Typical speciation diagrams are shown in Figure 1 for the two partial pressures of CO_2 (g) used for solution synthesis. Our reference aqueous samples included the major uranyl−carbonate complexes that may potentially exist under the oxic, neutral to weakly basic conditions commonly encountered at the Hanford site, a semiarid locale in south central Washington State. These conditions are representative of calcareous geochemical systems formed through the western United States. For comparison, one phosphate solution at much lower pH was also prepared. Due to the low solubility of most of the uranyl−phosphate complexes, thermodynamic calculation indicated that the only aqueous uranyl−phosphate complex with measurable concentration was $UO_2(HPO_4)_2^{2-}$ (Table 1).

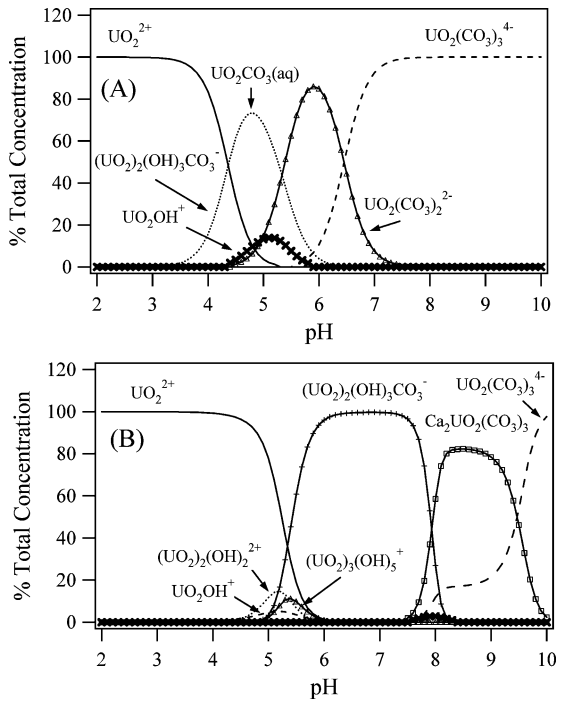

FIGURE 1. Typical speciation diagram for the aqueous uranyl−carbonates complexes: (A) partial pressure of CO_2 = 1 atm, total U(VI) = 2×10^{-6} M, I = 0.01 M $NaClO_4$ and (B) partial pressure of $CO_2 = 10^{-3.5}$ atm, total U(VI) = 1×10^{-5} M, $Ca^{2+} = 5 \times 10^{-3}$ M, I = 0.1 M $NaClO_4$.

Hanford Vadose Zone Porewater Samples. Porewaters were obtained by high-speed centrifugation of two, high moisture content (20 vol %), U(VI)-contaminated vadose zone sediments (55A and 61A) from Hanford's BX high level waste tank farm. Tank BX-102 experienced an overflow event in 1951 that released over seven metric tons of U(VI) to the vadose zone in the form of an 80 °C, 5.0 M $Na^+-HCO_3^-$ solution containing 0.5 M U(VI). A significant vadose zone U(VI) plume resulted from the spill. A borehole was installed next to tank BX-102 in 2002 to characterize the U(VI) concentration profile in the plume and to obtain samples for scientific study. Samples 55A and 61A were obtained from this borehole; they were retrieved from the near center of the mass of the plume at depths of 37.0 and 40 m, respectively. The chemical composition of these pore waters as measured by Serne et al. (*35*) is listed in Table 3.

Cryogenic U(VI) Fluorescence Measurements. Fluorescence spectroscopic and lifetime measurements were performed in a cryostat at liquid He-temperature as described elsewhere (*33*). Briefly, a small volume of the aqueous sample

TABLE 3. Uranyl and Major Chemical Components (M) in BX-102 Porewater Samples

component	55A	61A
UO_2^{2+}	2.81×10^{-3}	1.85×10^{-3}
K^+	1.23×10^{-3}	3.89×10^{-4}
Na^+	1.35×10^{-1}	5.31×10^{-2}
Ca^{2+}	9.53×10^{-4}	7.11×10^{-4}
Mg^{2+}	1.16×10^{-3}	1.90×10^{-4}
Cl^-	1.58×10^{-3}	4.51×10^{-4}
NO_3^-	3.35×10^{-2}	5.69×10^{-3}
SO_4^{2-}	1.56×10^{-2}	2.62×10^{-3}
PO_4^{3-}	3.45×10^{-3}	1.63×10^{-3}
H_4SiO_4	3.74×10^{-4}	7.16×10^{-4}
inorganic C	7.21×10^{-2}	4.11×10^{-2}
pH	9.3	9.06

was transferred into a 2 mm × 4 mm × 25 mm fused quartz cuvette under the atmosphere under which the sample was prepared, and the cuvette was capped with a silicone stopper and further sealed by wrapping the cuvette inlet with paraffin. Individual samples were attached to the coldfinger of a Cryo Industries RC-152 cryogenic workstation in which the sample cell was directly exposed to the vapor flow of liquid helium. Both the liquid helium flow rate and the electric current applied to the internal heater of the cryostat were tuned to achieve a stable temperature of 6 ± 1 K. The fluorescence emission spectra of the samples was obtained by excitation at either 415 nm using a Spectra-Physics Nd:YAG laser pumped MOPO-730 laser or at 375 nm using a Light Age Model 101 PAL alexandrite laser. The emitted light was collected at 75° to the excitation beam by a 2 in. diameter f/3 fused silica lens and focused by a 2 in f/4 fused silica lens into the entrance slit of an Acton SpectroPro 300i double monochromator spectrograph. For highly scattering samples, an Omega 460LP filter with a cutoff wavelength of 460 nm was placed in front of the spectrograph to reject scattered laser light. Prior tests have shown that excitation at either wavelength resulted in similar fluorescence spectra.

Time-resolved emission spectra were recorded using a thermoelectrically cooled Princeton Instruments PIMAX time-gated intensified CCD camera that was triggered by the delayed output of the laser pulse and controlled by the WinSpec data acquisition software. The same sample volume and geometry were maintained during analysis to allow semiquantitative analysis of the species distribution.

U(VI) fluorescence lifetimes were recorded by diverting the emitted light into a CVI model CM110 monochromator and detected by a Hamamatsu R928 photomultiplier tube (PMT) fitted with Hamamatsu C1392-57 time-gating PMT socket. The fluorescence intensity signal from the PMT was amplified and recorded with a Tektronix TDS 754A digital oscilloscope. Data analysis was performed using the commercial software package IGOR. Fluorescence decay analysis was performed with the Globals program developed at the UIUC (*36*).

Results and Discussion

Fluorescence Spectral Characteristics of Aqueous Uranyl−Carbonate/Phosphate Complexes. While aqueous uranyl displayed fluorescence spectra with appreciable intensity, none of the carbonate-bearing uranyl complex solutions showed any discernible fluorescence spectra at RT under the conditions of this work (Figure 2). In comparison, the uranyl phosphate solution showed well-resolved fluorescence spectra with moderate spectral intensity (Figure 2). The results for the phosphate complex were consistent with the observations of Brendler et al. (*26*).

The effect of temperature on the fluorescence spectra of the aqueous uranyl−carbonate complexes was dramatic

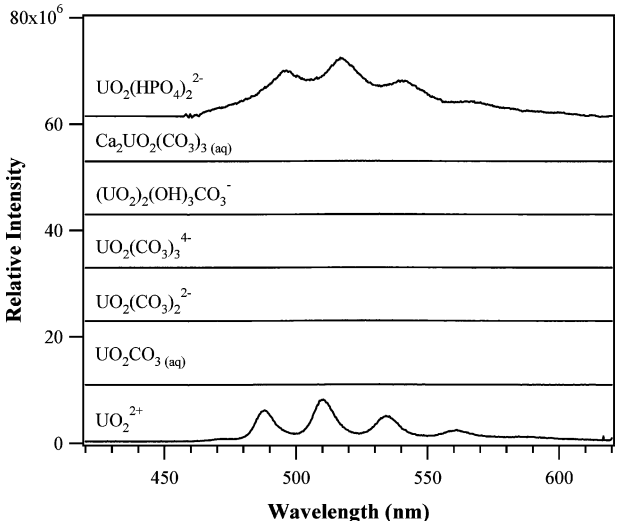

FIGURE 2. Fluorescence spectra of the aqueous uranyl−carbonate/phosphate complexes at RT. The detailed solution compositions are given in Table 1. For clarity, the spectra were normalized to the same maximum intensities and offset along the vertical axis.

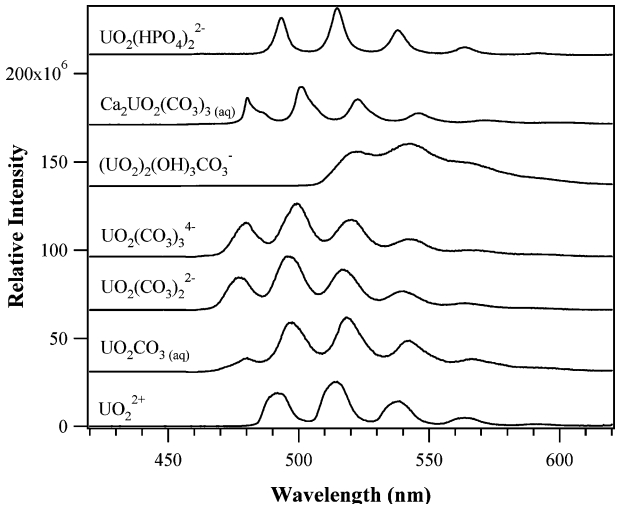

FIGURE 3. Fluorescence spectra of the aqueous uranyl−carbonate/phosphate complexes at 6 K. The detailed solution compositions are given in Table 1. For clarity, the spectra were normalized to the same maximum intensities and offset along the vertical axis.

(Figure 3). All uranyl−carbonate or mixed uranyl−carbonate complexes showed strong, well-resolved fluorescence spectra at LHeT (Figure 3). To our knowledge, this is the first observation of the fluorescence spectra of the $UO_2(CO_3)_2^{2-}$, $UO_2(CO_3)_3^{4-}$, and $(UO_2)_2(OH)_3CO_3^-$ complexes.

It is well-known that the thermodynamic stability of metal complex varies with temperature. Uranyl speciation at lower temperatures will be different from those calculated at room temperature. Because thermodynamic data for uranyl complexes at lower temperatures are nearly nonexistent, an accurate account of the uranyl speciation at LHeT in these solutions is impossible. For metal complexes whose enthalpy of formation ($\Delta H°$) is known, the stability constant at other temperatures can be estimated under the assumption that the heat capacity of the complex is constant, $\Delta C_p = 0$ (*37*, *38*), using the following linear relationship

$$\log(K_2) = \log(K_1) + \Delta H° (T_2 - T_1) * 0.00246 \qquad (1)$$

in which K represents stability constant and the subscripts 1 and 2 indicate the data at 25 °C and the temperature to be

TABLE 4. Fluorescence Spectral Characteristics of U(VI)−Carbonate Complexes, I = 0.1 M, λ_{ex} = 375 nm

major species	spectral maxima (nm)	ν_1(f)[d] (cm^{-1})	ν_1(vib)[a,e] (cm^{-1})	τ at LHe T (μs)	τ at RT (μs)
UO_2^{2+}(100%)	491.7, 513.9, 538.4, 563.5, 591.9	861	870[a]	270	1.8
UO_2CO_3(74%)	479, 498, 519, 542,567	810	851[a]	465, 39	*c*
$UO_2(CO_3)_2^{2-}$(86%)	477.4, 496.4, 517.2, 539.8, 563.5	800	834[b]	962, 70	*c*
$(UO_2)_2(OH)_3CO_3^-$(100%)	*c, c,* 523.0, 542.3, 561.3	652	834[b]	144	*c*
$UO_2(CO_3)_3^{4-}$(100%)	479.6, 499.2, 519.9, 542.4, 565.6	792	812[a]	883, 62	*c*
$Ca_2UO_2(CO_3)_3$(100%)	480.5, 501.2, 522.7, 546.0, 571.9	832	*c*	1282	*c*
$UO_2(HPO_4)_2^{2-}$(100%)	496.3, 516.8, 540.3, 566.8	835	*c*	564	47

[a] Data from ref *51*. [b] Data from ref *52*. [c] Not determined. [d] Uranyl totally symmetric stretching frequency, ν_1, determined by the average peaking spacing between the vibronic bands in the LHeT fluorescence spectra. [e] ν_1 determined from Raman spectra.

estimated, respectively. For uranyl complexes in this work, only the enthalpy data for UO_2CO_3 (aq), $UO_2(CO_3)_2^{2-}$, and $UO_2(CO_3)_3^{4-}$ are known (*39*). Using the compositional data for solution #4 (Table 1) in which the three binary uranyl−carbonate complexes constitute more than 99% of total uranyl, the stability constant data at 273 K obtained with eq 1, speciation calculations were performed. The results indicated that the percentage distribution of the major species, ($UO_2(CO_3)_2^{2-}$), only differed by 1% when the temperature was lowered from 298 K to at 273 K. Although we do not have estimates for the other solutions due to incomplete $\Delta H°$ values, we expect that any changes of the stability constants will not be large enough to alter the order of the distribution of the major complexes. It is also reasonable to assume that once the solutions were frozen, further lowering temperature to LHeT would only modify the speciation marginally.

The observed enhancement of fluorescence spectral intensity and resolution with temperature decrease was consistent with the observations of Becquerel et al. (*40*), Nichols and Howes (*41*), Samojlov (*42*), Dieke and Duncan (*43*), and our previous work with the uranyl silicates (*33*). The increased spectral resolution results from the reduction of the contributions of various vibrational modes related to the carbonate groups, the solvent water molecule, and phonons (*44*) as well as the suppression of any emission resulting from thermally populated vibrational levels in the excited electronic state (*45*, *46*). The intensity increase resulted from the elimination of energy loss facilitated by the vibrations that were suppressed at LHeT and the minimization of fluorescence quenching resulting from proton and electron transfer (*47*−*49*).

As shown in Figure 3, there were discernible spectral differences between the seven uranyl species at LHeT, making it possible to discriminate between them via their fluorescence spectroscopic signatures. Compared with the spectra of the aqueous uranyl ion which has a band origin (*50*) of 491.7 nm at LHeT, the spectra of $UO_2(HPO_4)_2^{2-}$, and especially that of $(UO_2)_2(OH)_3CO_3^-$, were largely red-shifted. The red-shift amounted to more than 40 nm for $(UO_2)_2(OH)_3CO_3^-$ (Table 4 and Figure 3). In contrast, all the uranyl−carbonate complexes were blue shifted toward shorter wavelengths. Additionally, there were appreciable differences in the spectral positioning of the individual vibronic peaks among the four uranyl−carbonate complexes (Table 4). The LHeT fluorescence spectral signatures of the uranyl−phosphate and −carbonate complexes were evidently dependent on their structures and compositions.

The dinuclear complex, $(UO_2)_2(OH)_3CO_3^-$, involves the bridging of the two uranyl ions by a hydroxide and/or a carbonate group and the coordination of both hydroxide groups and a carbonate in the equatorial plane (*53*). However, a spectral comparison of this complex with those of the other binary uranyl−carbonate complexes and uranyl oxyhydroxide minerals (*33*, *54*) indicated that the $(UO_2)(OH)_3CO_3^-$ complex exhibited the spectral signature of an oxyhydroxide.

Besides the spectral variations among the complexes, there were significant differences in the fluorescence lifetimes and the spacing between the resolved vibronic peaks of the different complexes. The latter effect resulted from the coupling of the electronic transition with the totally symmetric stretch frequency of the linear O═U═O ion. At 6 K, the fluorescence lifetimes of the uranyl−carbonate complexes varied from 144 μs for $(UO_2)(OH)_3CO_3^-$ to 1.282 ms for $Ca_2UO_2(CO_3)_{3(aq)}$. The lifetimes were dependent on the composition and stoichiometry of the complex. Generally, the coordination of hydroxide groups and the presence of inner-sphere waters, such as in UO_2^{2+}, $UO_2CO_{3(aq)}$, and $(UO_2)_2(OH)_3CO_3^-$, reduced the observed fluorescence lifetime. The fluorescence lifetime of $UO_2(CO_3)_3^{4-}$ was slightly shorter than that of $UO_2(CO_3)_2^{2-}$ and noticeably shorter than $Ca_2UO_2(CO_3)_{3(aq)}$, suggesting that other structural and compositional factors influenced fluorescence lifetime. The numerical fitting of the fluorescence decays of all three binary uranyl−carbonate complexes required the inclusion of a minor component with much shorter fluorescence lifetime. A similar observation was made for uranyl silicate minerals at 6 K (*33*). It is not known whether this component is a real entity or an artifact of other factors.

The enhanced spectra resolution allowed more accurate calculation of the O═U═O symmetrical stretch frequency, ν_1, that corresponds to the average spacing of the vibronic peaks of the fluorescence spectra as compared to that at RT. For uranyl compounds, this frequency is inversely correlated to the strength of the interaction of U(VI) with the coordinating ligand in the equatorial plane. A stronger interaction between U(VI) and the equatorial ligand results in weaker apical U═O bond and thus a lower O═U═O stretching frequency (*52*). The calculated ν_1 values varied from 861 cm^{-1} for the aqueous uranyl ion to 652 cm^{-1} for $(UO_2)_2(OH)_3CO_3^-$. For the three binary uranyl−carbonate complexes, the ν_1 values showed gradual decrease from 810 cm^{-1} for $UO_2CO_{3(aq)}$, to 792 cm^{-1} for $UO_2(CO_3)_3^{4-}$. Clearly, carbonate complexation caused a decrease in the symmetrical stretching frequency of uranyl. As noted previously, the small ν_1 value for the $(UO_2)_2(OH)_3CO_3^-$ complex was similar to the uranyl oxyhydroxides (*33*) and some of the uranate salts (*55*, *56*).

Calculating the ν_1 values of uranyl complexes from fluorescence spectra offers a complemental method to Raman and infrared (IR) spectroscopy for compounds where the molecular symmetry has been lowered from point group $D_{\infty h}$ (*57*). The concentration of uranium in most natural waters is below the detection limit of Raman and IR (approximately 0.1% [w/w]) and, thus, fluorescence spectroscopy becomes the only way to obtain this structurally important information. However, it should be noted that the ν_1 values obtained from the fluorescence spectra are often smaller than those obtained from Raman or IR (Table 4). For example, the ν_1 values for the aqueous uranyl ion and $UO_2(CO_3)_3^{4-}$ as measured by Raman spectroscopy are 870 and 812 cm^{-1}, respectively (*51*). The ν_1 values for these same complexes as measured by fluorescence spectroscopy are 861 and 792 cm^{-1}. Such

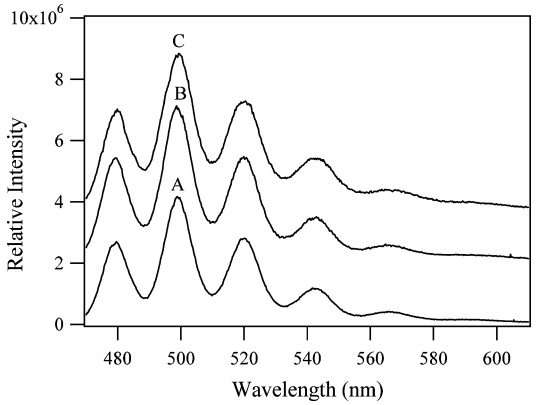

FIGURE 4. Fluorescence spectra of the vadose zone porewater samples at 6 K: (A) 55A and (B) 61A. The spectra of $UO_2(CO_3)_3^{4-}$ (C) is included for comparison. For clarity, all spectra are normalized and curves (B) and (C) are offset along the vertical axis.

TABLE 5. Fluorescence Spectral Characteristics of U(VI) in Pore Waters of Hanford Sediments, λ_{ex} = 415 nm

sample	spectral maxima (nm)	ν_1 (f)[b] (cm^{-1})	ν_1(vib)[c] (cm^{-1})	τ at He T (μs)	τ at RT (μs)
55A	479.6, 498.8, 520.1, 542.1, 566.8	803.9	*a*	883	*a*
61A	479.7, 498.8, 519.9, 542.7, 566.8	810.9	*a*	869	*a*

[a] Not determined. [b] Uranyl totally symmetric stretching frequency, ν_1, determined by the average peaking spacing between the vibronic bands in the LHeT fluorescence spectra. [c] ν_1 determined from Raman spectra.

differences may result from the fact that Raman spectroscopy only measures the symmetrical vibration frequency. In contrast, the vibronic bands in the fluorescence spectra include contributions from other lower frequency vibration modes (*44*) that reduce the overall spacing between the vibronic bands. Error in the determination of the vibronic peak positions in the fluorescence spectra can also be larger than with Raman or IR spectroscopies because of the relative broadness of the vibronic bands in the fluorescence spectra.

Fluorescence Spectra of Hanford Vadose Zone Porewaters at RT and LHeT. The 55A and 61A porewaters from the Hanford vadose zone sediments showed little fluorescence at RT even though the total U(VI) concentrations were as high as 2.81×10^{-3} M (Table 3). Once the sample temperature was lowered to 6 K, both samples displayed strong, well-resolved uranyl fluorescence spectra (Figure 4). Although the two samples were obtained at depth levels that were 2 m apart, their fluorescence spectra were essentially identical, implying similar U(VI) speciation in the porewaters of these sediments.

The fluorescence spectral profiles, vibronic peak positions, fluorescence lifetimes, and the symmetric O=U=O stretching frequencies of the sediment porewaters matched most closely with the uranyl−tricarbonate complex, $UO_2(CO_3)_3^{4-}$ (Figure 3 and Tables 4 and 5), although small differences were noted. The fluorescence lifetimes, 883 μs and 869 μs for 55A and 61A, respectively, were in good agreement with that of the $UO_2(CO_3)_3.^{4-}$ Similarly, the ν_1 values of the 55A and 61A pore waters, 803.9 and 810.9 cm^{-1}, were only slightly larger than that of the $UO_2(CO_3)_3^{4-}$ complex. The minor variations among these data may indicate the presence of a small fraction of other component, such as the $Ca_2UO_2(CO_3)_{3(aq)}$ species. Also, it should be pointed out that the porewaters contain high concentrations of Fe and Al. Although these solutions were clear under visual inspection, at pH above 9, there was always the possibility that small colloids might form (*58*). Such colloids might affect the speciation of uranyl ion by adsorption and coprecipitation. However, due to the high carbonate concentration and the high thermodynamic stability of uranyl−carbonate complexes, such effect, if exists, is likely minimal.

TABLE 6. Uranyl Speciation (mol/L) of Porewater from BX-102[a]

species	55A	61A
$UO_2(OH)_{2(aq)}$	2.36×10^{-12}	2.13×10^{-11}
$UO_2(OH)_3^-$	2.34×10^{-11}	9.88×10^{-11}
$UO_2CO_{3(aq)}$	6.32×10^{-12}	8.33×10^{-11}
$UO_2(CO_3)_2^{2-}$	5.81×10^{-7}	2.20×10^{-6}
$UO_2(CO_3)_3^{4-}$	2.79×10^{-3} (99.3%)	1.79×10^{-3} (96.5%)
$Ca_2UO_2(CO_3)_{3(aq)}$	1.88×10^{-5} (0.7%)	6.11×10^{-5} (3.4%)
$UO_2PO_4^-$	2.80×10^{-12}	3.17×10^{-11}
total	2.81×10^{-3}	1.85×10^{-3}

[a] Number in bracket is the species percentage of total uranyl concentration in the sample; no solid phase was allowed to precipitate or dissolve; species at concentrations less than 10^{-12} M are omitted.

U(VI) aqueous speciation was calculated for the porewater samples (Table 6). The calculation employed MINTEQ-A2 and the best available thermodynamic data (Table 2). The results of the calculation (Table 6) indicated that the $UO_2(CO_3)_3^{4-}$ was indeed the dominant U(VI) species in these porewaters, albeit small variations did exist among the three samples because of differences in pH and composition. The relative amount of $UO_2(CO_3)_3^{4-}$ was between 99.3% for 55A to 96.5% for 61A, while the remainder was present as $Ca_2UO_2(CO_3)_{3(aq)}$. In contrast, Kohler et al. (*59*) found that calcium uranyl−carbonate complexes dominated the aqueous speciation of groundwaters from Naturita Colorado that had been contaminated by seepage from uranium mine mill tailings. The aqueous speciation calculations were in complete agreement with the conclusions of the fluorescence measurements.

Our reference "aqueous species" standards contained only one uranyl phosphate complex that formed at low pH, and its fluorescence spectrum (Figure 3) was clearly different from those of the porewaters at both RT and LHeT (Figure 4). Considering the relatively high pH of the porewaters, the presence of other uranyl−phosphate or mixed ligand uranyl complexes with phosphate and hydroxide (*26*) with appreciable concentration does not seem probable, as demonstrated by the speciation modeling (Table 6). Although, our reference solutions did not contain examples of silicate complexes, reference spectra for these complexes at RT have been published (*25*) and the corresponding thermodynamic data have been reported (*25*). Neither the LIF spectra (Figure 4) or the results of the thermodynamic calculations (Table 6) showed evidence for aqueous uranyl−silicate complexes, despite the presence of precipitated uranyl silicates in sediments (*8*, *60*). The higher order U(VI)−carbonate complexes appeared to be the mobile species responsible for the subsurface migration of U(VI) at this particular Hanford site, while the majority of the in-ground U inventory existed in the form of U(VI)−silicate precipitates (uranophane or boltwoodite).

Our results were consistent with fluorescence spectroscopic measurements of U(VI) speciation made by Bernhard et al. (*7*, *14*) in European mine discharge waters. These authors found that the spectral and lifetime characteristics of U(VI) in neutral, high Ca (11.5 mM) seepage waters were consistent with $Ca_2UO_2(CO_3)_{3(aq)}$. Higher pH (9.68) mine seepage waters with lower Ca (0.3 mM) yielded fluorescence results indicative of $UO_2(CO_3)_3.^{4-}$ Although porewaters in the Hanford vadose zone are generally in equilibrium with calcite, their com-

position is similar to the higher pH mine waters of Bernhard et al. (*7*, *14*). The uranyl−tricarbonate complex appears as the dominant U(VI) species in waters of that composition both by thermodynamic calculation and fluorescence measurement.

Sediment pore waters offer a critical link between the leaked tank waste streams and the current chemical state and migration behavior of U(VI) in the sediment. The current composition of the porewaters reflects the progress of a complicated reaction network that has occurred between the leaked waste solution and sediment minerals over the past 50 years. The pore water concentrations of U(VI) and its speciation reflects the energetics of different U(VI) phases and phase associations and the impact of other waste-derived and endogenous chemical components. The U(VI) species in such porewaters signify those that may be actively migrating in soils and sediments.

In this study, we have directly observed that the $UO_2(CO_3)_3^{4-}$ complex is the major aqueous species in U(VI)-contaminated sediment that contains precipitated uranyl silicates in the grain interiors of plagioclase minerals. The reaction network and associated hydrologic factors responsible for the uranyl silicate precipitation have not yet been resolved and are under investigation. Field observations indicate that mobile U(VI) is migrating through the vadose zone to groundwater at this site (*61*), and our measurements indicate that the tricarbonate complex is the mobile species. Carbonate complexation reduces uranyl adsorption by iron oxides (*17*, *62*−*64*), subsurface materials (*65*), and aquifer sediments (*66*). Spectroscopic measurements have shown that carbonate complexes may adsorb to mineral surfaces, albeit weakly (*5*, *67*). Further measurements are needed on deep vadose zone materials from Hanford to understand the extent to which these complexes adsorb to the Fe(III)−oxide poor mineral suite at this site (*68*) and the resulting retardation factors.

Acknowledgments

The authors thank Dr. L. Rao at Berkeley National Laboratory for helpful discussions about f-element thermodynamics at variable temperatures. The manuscript has been greatly improved with the suggestions and comments of three anonymous reviewers. This project was supported by the Hanford Remediation and Closure Science Project and by the Environmental Management Sciences Program (EMSP) managed by the U.S. DOE Office of Biological and Environmental Research (OBER). The fluorescence measurements were performed at the W.R. Wiley Environmental Molecular Sciences Laboratory, a national scientific user facility managed by the Department of Energy's Office of Biological and Environmental Research and located at PNNL. Pacific Northwest National Laboratory is operated for the Department of Energy by Battelle Memorial Institute.

Literature Cited

(1) Grenthe, I.; Konings, R. J. M. *Chemical Thermodynamics of Uranium*; Wanner, H., Ed.; 1992; Elsevier: North-Holland.

(2) Kato, Y.; Meinrath, G.; Kimura, T.; Yoshida, Z. *Radiochim. Acta* **1994**, *64*, 107−111.

(3) Burns, P. C. *The Crystal Chemistry of Uranium*. In *Reviews in Mineralogy, Uranium: Mineralogy, Geochemistry and the Environment*; Burns, P. C., Finch, R., Eds.; Mineralogical Society of America: Washington, DC, 1999; pp 24−90.

(4) Finch, R.; Murakami, T. *Systematics and Paragenesis of Uranium Minerals*. In *Reviews in Minerology, Uranium: Mineralogy, Geochemistry and the Environment*; Burns, P. C., Finch, R., Eds.; Mineralogical Society of America: Washington, DC, 1999; pp 91−179.

(5) Bargar, J. R.; Reitmeyer, R.; Lenhart, J. J.; Davis, J. A. *Geochim. Cosmochim. Acta* **2000**, *64*, 2737−2749.

(6) Kim, J. I. *Chemical Behavior of Transuranic Elements in Natural Aquatic Systems*, in *Handbook on the Physics and Chemistry of the Actinides*; 1986.

(7) Bernhard, G.; Geipel, G.; Brendler, V.; Nitsche, H. *J. Alloys Compd.* **1998**, *271*−*273*, 201−205.

(8) Liu, C.; Zachara, J. M.; Q. O., McKinley, J. P.; Heald, S. M.; Wang, Z. *Geochim. Cosmochim. Acta*, **2003**, Submitted.

(9) Bostick, B. C.; Fendorf, S.; Barnett, M. O.; Jardine, P. M.; Brooks, S. C. *Soil Sci. Soc. Am. J.* **2002**, *66*, 99−108.

(10) Kaplan, D. I.; Gervais, T. L.; Krupka, K. M. *Radiochim. Acta* **1998**, *80*, 201−211.

(11) Arey, J. S.; Seaman, J. C.; Bertsch, P. M. *Environ. Sci. Technol.* **1999**, *33*, 337−342.

(12) Jerden, J. L., Jr.; Sinha, A. K.; Zelazny, L. *Chem. Geol.* **2003**, *199*, 129−157.

(13) Geipel, G.; Bernhard, G.; Rutsch, M.; Brendler, V.; Nitsche, H. *Radiochim. Acta* **2000**, *88*, 757−762.

(14) Bernhard, G.; Geipel, G.; Brendler, V.; Nitsche, H. *Radiochim. Acta* **1996**, *74*, 87−91.

(15) Morris, D. E.; Allen, P. G.; Berg, J. M.; Chisholm-Brause, C. J.; Conradson, S. D.; Donohoe, R. J.; Hess, N. J.; Musgrave, J. A.; Tait, C. D. *Environ. Sci. Technol.* **1996**, *30*, 2322−2331.

(16) Payne, T. E.; Davis, J. A.; Waite, T. D. *Radiochim. Acta* **1996**, *74*, 239−243.

(17) Waite, T. D.; Davis, J. A.; Payne, T. E.; Waychunas, G. A.; Xu, N. *Geochim. Cosmochim. Acta* **1994**, *58*, 5465−5478.

(18) Davis, J. A.; Coston, J. A.; Kent, D. B.; Fuller, C. C. *Environ. Sci. Technol.* **1998**, *32*, 2820−2828.

(19) Rogers, J. J. W.; Adams, J. A. S. *Uranium*. In *Handbook of Geochemistry*; Wedepoh, K. H., Ed.; Springer: New York, 1972; Vol. 2, Chapter 92 B.

(20) Geipel, G.; Bernhard, G.; Brendler, E.; Nitsche, H. *Radiochim. Acta* **1998**, 82, 59−62.

(21) Beitz, J. V.; Bowers, D. L.; Doxtader, M. M.; Maroni, V. A.; Reed, D. T. *Radiochim. Acta* **1988**, *44/45*, 87.

(22) Denning, R. G. *Struct. Bond.* **1992**, *79*, 215−276.

(23) Meinrath, G. *J. Radioanal. Nucl. Ch.* **1997**, *224*, 119−126.

(24) Geipel, G.; Brachmann, A.; Brendler, V.; Bernhard, G.; Nitsche, H. *Radiochim. Acta* **1996**, *75*, 199−204.

(25) Moll, H.; Geipel, G.; Brendler, V.; Bernhard, G.; Nitsche, H. *J. Alloy Compd.* **1998**, *271*, 765−768.

(26) Brendler, V.; Geipel, G.; Bernhard, G.; Nitsche, H. *Radiochim. Acta* **1996**, *74*, 75−80.

(27) Moulin, C.; Decambox, P.; Moulin, V.; Decaillon, J. G. *Anal. Chem.* **1995**, *67*, 348−353.

(28) Meinrath, G.; Lis, S.; Stryla, Z.; Noubactep, C. *J. Alloy Compd.* **2000**, *300*−*301*, 107−112.

(29) Baes, C. F. J.; Meyer, N. J. *Inorg. Chem.* **1962**, *1*, 780−789.

(30) Kalmykov, S. N.; Choppin, G. R. *Radiochim. Acta* **2000**, *88*, 603−606.

(31) Balzani, V.; Bolleta, F.; Gandolfi, M. T.; Maestri, M. *Top. Curr. Chem.* **1978**, *75*, 1−64.

(32) Bernhard, G.; Geipel, G.; Reich, T.; Brendler, V.; Amayri, S.; Nitsche, H. *Radiochim. Acta* **2001**, *89*, 511−518.

(33) Wang, Z.; Zachara, J. M.; Gassman, P. L.; Joly, A. G.; Liu, C. X.; Catalano, J. *Fluorescence Spectroscopic Studies of Uranium-Bearing Vadoze Zone Sediments, in Digest of Science and Technology Program Evaluation;* Hanford Vadoze Zone Report, RPP-10098; Pacific Northwest National Laboratory: Richland, WA, 2003.

(34) Porter, R. A.; Weber, W. J. *J. Inorg. Nucl. Chem.* **1971**, *33*, 2443−2449.

(35) Serne, J. R.; Brown, C. F.; Schaef, H. T.; Pierce, E. M.; Lindberg, M. J.; Wang, Z.; Gassman, P. L.; Catalano, J. G. *300 Area Uranium Leach and Adsorption Project*; PNNL-14022; Pacific Northwest National Laboratory: Richland, WA, 2002.

(36) Beechem, J. M.; Gratton, E.; Mantulin, W. W. *Globals Unlimited*; UIUC: Urbana, IL, 1991.

(37) Zanonato, P. L.; Di Bernardo, P.; Bismondo, A.; Rao, L.; Choppin, G. R. *J. Soln. Chem.* **2001**, *30*, 1−18.

(38) Martell, R. E.; Smith, R. M. *Critical Stability Constants of Metal Complexes database, Version 2;* NIST Standard Reference Data program, Gaithersburg, MD, 1995.

(39) Grenthe, I.; Fuger, J.; Konings, R. J. M.; Lemire, R. J.; Muller, A. B.; Nguyen, C.-T.; Wanna, H. *Chemical Thermodynamics. Vol. 1. Chemical Thermodynamics of Uranium. OECD-NEA*; Elsevier: The Netherlands, 1992.

(40) Becquerel, H.; Becquerel, J.; Onnes, H. K. *Ann. Chim. Phys. 8* **1910**, *20*, 145.

(41) Nichols, E. L.; Howes, H. L.; Wick, F. G. *Phys. Rev.* **1919**, *XIV*, 201−221.

(42) Samojlov, B. N. *Zh. Eksptl. Teoret. Fiz.* **1948**, *18*, 1030−1040.

(43) Dieke, G. H.; Duncan, A. B. F. *Spectroscopic Properties of Uranium Compounds*, in *National Nuclear Energy Series Div. III 2*; McGraw-Hill: New York, 1949.
(44) Rabinowitch, E.; Belford, R. L. *Spectroscopy and Photochemistry of Uranyl Compounds*; Pergaman Press: The MacMillan Company: New York, 1964.
(45) Bell, J. T. *J. Mol. Spec.* **1972**, *41*, 409−411.
(46) Tits, J.; Stumpf, T.; Babung, T.; Wieland, E.; Fanghänel, T. *Environ. Sci. Technol.* **2003**, *37*, 3568−3573.
(47) Stepanov, A. V.; Preobrazhenskaya, E. B.; Nikitina, S. A. *Radiokhmiya* **1984**, *26*, 798−803.
(48) Matsushima, R., F. H.; Sakuraba, S. *J. Chem. Soc., Faraday Trans.* **1974**, *72*, 1702−1709.
(49) Baird, C. P.; Kemp, T. J. *Prog. React. Kinet.* **1997**, *22*, 87−139.
(50) Meinrath, G.; Kato, Y.; Kimura, T.; Yoshida, Z. *Radiochim. Acta* **1998**, *82*, 115−120.
(51) Nguyen-Trung, C.,; Begun, G. M.; Palmer, D. A. *Inorg. Chem.* **1992**, *31*, 5280−5287.
(52) Maya, L.; Begun, G. M. *J. Inorg. Nucl. Chem.* **1981**, *43*, 2827−2832.
(53) Szabo, Z.; Moll, H.; Grenthe, I. *J. Chem. Soc., Dalton* **2000**, 3158−3161.
(54) Perry, D. L.; Brittain, H. G. *Inorg. Chem.* **1984**, *23*, 1232−1237.
(55) Volkovich, V. A.; Griffiths, T. R.; Thied, R. C. *Vib. Spectrosc.* **2001**, *25*, 223−230.
(56) Liegeois-Duyckaerts, M. *Spectrochim. Acta* **1977**, *33A*, 709−713.
(57) Cejka, J. *Infrared Spectroscopy and Thermal Analysis of the Uranyl Minerals.* In *Reviews in Minerology, Uranium: Mineralogy, Geochemistry and the Environment*; Burns, P. C., Finch, R., Eds.; Mineralogical Society of America: Washington, DC, 1999; pp 521−622.
(58) Kim, J. I. *Radiochim. Acta* **1991**, *52/53*, 71−81.
(59) Kohler, M. S.; Curtis, G.; Meece, D.; Davis, J. *Environ. Sci. Technol.* **2004**, *38*, 240−247.
(60) McKinley, J. P.; Zachara, J. M.; Liu, C.; Heald, S. M. *Nature* **2003**, Submitted.
(61) Christensen, J. N.; Dresel, P. E.; Conrad, M. E.; Maher, K.; DePaolo, D. J. *Environ. Sci. Technol.* **2003**, Submitted.
(62) Hsi, C. D.; Langmuir, D. *Geochim. Cosmochim. Acta* **1985**, *49*, 1931−1941.
(63) Duff, M. C.; Amrhein, C. *Soil Sci. Soc. Am. J.* **1996**, *60*, 1393−1400.
(64) Villalobos, M.; Trotz, M. A.; Leckie, J. O. *Environ. Sci. Technol.* **2001**, *35*, 3849−3856.
(65) Barnett, M. O.; Jardine, P. M.; Brooks, S. C. *Environ. Sci. Technol.* **2002**, *36*, 937−942.
(66) Davis, J.; Curtis, G.; Kohler, M. S.; Fox, P.; Meece, D. *Geochim. Cosmochim. Acta* **2003**, *67*, A76-A76 Suppl. 1.
(67) Bargar, J. R.; Reitmeyer, R.; Davis, J. A. *Environ. Sci. Technol.* **1999**, *33*, 2481−2484.
(68) Zachara, J. M.; Smith, S. C.; Liu, C. X.; McKinley, J. P.; Serne, R. J.; Gassman, P. L. *Geochim. Cosmochim. Acta* **2002**, *66*, 193−211.

Received for review March 30, 2004. Revised manuscript received July 16, 2004. Accepted August 16, 2004.

ES049512U